On the fabric tensor of polydisperse granular materials in 2D

Mahyar Madadi [a,b] Olivier Tsoungui [a] Marc Lätzel [a]
Stefan Luding [a,c,d]

[a] *Institute for Computational Physics, Pfaffenwaldring 27, 70569 Stuttgart, GERMANY*

[b] *Institute for Advanced Studies in Basic Sciences, Gaveh Zang, Zanjan, IRAN*

[c] *Particle Technology, DelftChemTech, Julianalaan 136, 2628 BL Delft, NETHERLANDS*

[d] *e-mail:* lui@ica1.uni-stuttgart.de *and:* s.luding@tnw.tudelft.nl

Abstract

The trace of the *fabric tensor* in static, isotropic, two-dimensional, frictionless, polydisperse granular materials is examined theoretically and numerically. In the monodisperse case, the trace of the fabric tensor equals the product of volume fraction and coordination number – thus the fabrics trace can be seen as contact density. For various size distributions, we obtain a correction factor to the monodisperse observation, which involves the first three moments of the particle size distribution function. The theoretical prediction is found to be in good agreement with numerical simulations of static frictionless systems.

Key words: Fabric tensor, discrete element simulation, bidisperse and polydisperse size distributions

1 Introduction

Inhomogeneous and anisotropic materials attract still increasing interest, not only in the framework of classical disordered systems like glasses but also, more recently, in connection to granular materials, see (Roux et al., 1987; Guyon et al., 1990; Vardoulakis and Sulem, 1995; Jaeger et al., 1996; Wolf and Grassberger, 1997; Herrmann and Luding, 1998; Vermeer et al., 2001). Disordered materials can be characterized by frozen-in or quenched disorder, a property that distinguishes them from a crystal, where long-range order exists, or a

simple fluid or gas, where homogeneity and isotropy can often be assumed. Connected to the structure of disordered materials, and of more general relevance, are concepts like rigidity percolation, see (Moukarzel, 1996; Jacobs, 1998), or internal variables to describe damage/fracture, see (Cambou and Sidoroff, 1985; Vardoulakis et al., 1998; Kun and Herrmann, 2000). Research focusses on the relations between the quantities stress, strain, and fabric, see (Cowin, 1985; Sadegh et al., 1991; Roux et al., 1991; Darve et al., 1995), and very recently a tremendous interest in homogenization and constitutive laws in the framework of a micro-macro transition emerged, see (Vermeer et al., 2001; Darve et al., 1995; Cambou et al., 1995; Emeriault and Chang, 1997; Cowin, 1998; Kuhl et al., 2000; Ehlers and Müllerschön, 2000; Dedecker et al., 2000; Oda and Iwashita, 2000; Bagi, 1996, 1999; Edwards and Grinev, 1999; Ball and Blumenfeld, 2002; Bagi, 2003). A helpful tool for such studies are discrete element or, with other words, molecular dynamics simulation techniques, as introduced by Cundall and Strack (1979, 1983); Allen and Tildesley (1987), and applied to idealized granular materials by Radjai et al. (1999); Lätzel et al. (2000); Luding et al. (2001a,b); Luding and Herrmann (2001); Lätzel et al. (2001); Luding (2002a).

An essential question is the characterization of disorder and, as a first step, the quantitative prediction of mean material properties. Straightforward progress is possible when a periodic structure (crystal) is regarded: one has only to account for one unit cell and global properties can easily be predicted, as done by Kruyt and Rothenburg (2001); Luding and Herrmann (2001); Luding (2004). For disordered media, the concept of the fabric tensor naturally occurs when the system consists of an elastic network, or a packing of discrete particles. The fabric tensor is then a zero- and second-order harmonic fit to the probability distribution function for load-carrying contacts in a given direction.

Various definitions of the fabric tensor exist in the literature, see (Rothenburg and Selvadurai, 1981; Goddard, 1986; Mehrabadi et al., 1988; Chang, 1988; Thornton and Randall, 1988), including definitions for elliptical or polygonal particles, see (Sadd et al., 1997; Goddard, 1998), and tensors of higher rank than two, see (Chang et al., 1995; Jenkins, 1997; Tobita, 1997). The fabric tensor can be related to the anisotropic material stiffness tensor, see (Bathurst and Rothenburg, 1988; Chang et al., 1995; Kruyt and Rothenburg, 1996; Liao and Chang, 1997; Liao et al., 1997; Bigoni and Loret, 1999; Bagi, 1999), in static, frictionless assemblies. The isotropic part, i.e. the trace of the fabric is then a measure for the bulk stiffness or compressibility under isotropic strain, see (Lätzel et al., 2000; Luding, 2002a). The fabric is most readily examined by means of molecular dynamics simulations, as done by Cundall and Strack (1983); Thornton (1997); Luding (1997); Thornton (2000); Thornton and Antony (2000); Oda and Iwashita (2000), but also experiments are available, see for example (Oda et al., 1997; Dubujet and Dedecker, 1998; Tsoungui et al., 1998).

The dynamical evolution of the fabric tensor, as examined by Shima (1993); Kruyt and Rothenburg (2001) during compaction, by Dubujet and Dedecker (1998) during constant volume deformation, by Oda et al. (1997); Oda and Kazama (1998); Thornton (2000); Thornton and Antony (2000); Oda and Iwashita (2000); Kruyt and Rothenburg (2001) during shear, and by Luding (1997) for various boundary conditions, is still an open issue; see also (Roux, 1997, 2000). The inclusion of the concept of a dynamic material structure tensor into continuum models (Dubujet and Dedecker, 1998) or its relation to advanced hypoplastic continuum constitutive models, see (Kolymbas et al., 1995; Bauer and Tejchman, 1995; Gudehus, 1996; Tejchman, 2002), with internal tensorial state variables.

The purpose of this paper is to examine the isotropic part of the fabric tensor in static, isotropic, two-dimensional (2D), polydisperse packings, as a first step. Throughout this paper a volume can also be seen as an area and a particle surface can be interpreted as the circumference of a particle. After the definition of the fabric used here, the effect of different particle size distributions on the fabric tensor is examined theoretically. The solution of our approach is then approximated (in order to allow for simpler equations) and compared to numerical simulations of corresponding assemblies with different particle size distribution functions.

2 Single particle case

One quantity that describes the local configuration of a granular assembly to some extent is the fabric tensor of second order

$$F^p_{\alpha\beta} = \frac{1}{a_p^2} \sum_{c=1}^{C^p} l^{pc}_\alpha l^{pc}_\beta \ , \quad \text{with} \ \ l^{pc}_\alpha = a_p \ n^c_\alpha \ , \tag{1}$$

where the n^c_α are the components of the unit normal vector at contact c of particle p with radius a_p. Eq. (1) is a definition of the fabric tensor that uses the so-called branch vector $\vec{l}^{pc}$ from the center of particle p to its contact c. However, the unit normal and the unit branch vector are identical in the case of spherical particles (disks in 2D). The trace of the fabric tensor,

$$F^p_{\alpha\alpha} = \sum_{c=1}^{C^p} n^c_\alpha n^c_\alpha = C^p \ , \tag{2}$$

is the number of contacts of the particle, C^p.

3 Many particle case

The mean fabric tensor is a quantity that describes the contact network in a given volume V. The three-dimensional volume is obtained from the two-dimensional area by multiplication with the length of the system (height of the disks), h. Thus we continue with the expression volume, because the formalism can easily be extended to three dimensions. Assuming that all particles which lie inside V contribute to the fabric with a weight $V_p = \pi h a^2$, we take the average of the fabric tensor by weight V_p

$$\langle F_{\alpha\beta} \rangle_V = \frac{1}{V} \sum_p V_p F^p_{\alpha\beta} \ . \tag{3}$$

There would be at least two possibilities for V_p: (*i*) the volume of the polygon (e.g. obtained via a Voronoi tesselation) that contains the particle, or (*ii*) the volume of the particle itself. We choose option (*ii*) so that in analogy to the trace of the fabric for a single particle, the trace of the averaged fabric is

$$\langle F_{\alpha\alpha} \rangle_V = \frac{\pi h}{V} \sum_{p \in V} a_p^2 \ C^p \tag{4}$$

$$= \frac{1}{V} \sum_p V_p C^p \ , \tag{5}$$

a contact number density – in our definition. Alternative definitions, (Cowin, 1985; Goddard, 1986; Chang, 1988; Sadegh et al., 1991; Dubujet and Dedecker, 1998; Cowin, 1998; Bigoni and Loret, 1999), see may involve constant prefactors or slightly different contributions, e.g. the connection vector from particle-center to its contact neighbors center can be used, so that our interpretation may not be applicable.

3.1 Monodisperse particles

In the monodisperse case, Eq. (4) for identical particles ($a_p = a$) reduces to $\langle F_{\alpha\alpha} \rangle_V = \nu \langle C \rangle$, where ν is the volume fraction, defined as the ratio of the volume covered by particles and the total volume. This is because in 2D, the system arranges itself in an almost regular, periodic triangular lattice. The brackets $\langle ... \rangle$ denote an average by particle, i.e. $\langle C \rangle = (1/N) \sum_p C^p$, whereas $\langle ... \rangle_V$ denotes an average by volume-weight, see Eq. (3). The volume fraction is thus defined as $\nu = \langle 1 \rangle_V$.

The situation is different for a polydisperse granular packing, insofar as Eq. (4) does not reduce to $\langle F_{\alpha\alpha}\rangle_V = \nu\overline{C}$. The principal problem is to evaluate the sum in Eq. (4) as a function of the size distribution.
Assume a polydisperse distribution of particle radii with probability $f(a)\ da$ to find the radius a between radii a and $a + da$, and with $\int_0^\infty\ da\ f(a) = 1$. Therefore considering the continuous limit of Eq. (5), one has:

$$\langle F_{\alpha\alpha}\rangle_V = \frac{N}{V}\int_0^\infty da\ V_p(a)\ C(a)\ f(a)\ , \tag{6}$$

with the mean number of contacts $C(a)$ of particles with radius a. With a continuous size distribution function, the volume fraction is obtained via

$$\nu = \langle 1\rangle_V = \frac{N}{V}\int_0^\infty da\ V_p(a) f(a)\ . \tag{7}$$

We will evaluate Eq. (6) using an approach similar to the one proposed by Ouchiyama and Tanaka (1981). Assume that a reference particle with radius a is surrounded by identical particles of mean radius $\overline{a}$ where $\overline{a} = \int_0^\infty\ da\ a\ f(a)$. Here we are interested in that part of the reference particle's surface that is covered or shielded by a contact partner, as sketched in Fig. 1.

The surface angle covered by a particle with radius $\overline{a}$ on a particle of radius a is

$$2\phi(a) = 2\arcsin\left(\frac{\overline{a}}{a+\overline{a}}\right) = 2\arcsin\left(\frac{1}{2+\epsilon}\right)\ , \tag{8}$$

where $\epsilon = a/\overline{a} - 1$ is a small quantity for narrow size distributions and thus quantifies the deviation from the monodisperse situation.

The linear compacity

$$c_s = 2\phi(a)C(a)/2\pi \tag{9}$$

of the reference particle is defined as the fraction of its surface which is shielded by other particles. Now, the basic assumption is that c_s is independent of a or, with other words, the number of contacts is proportional to the surface

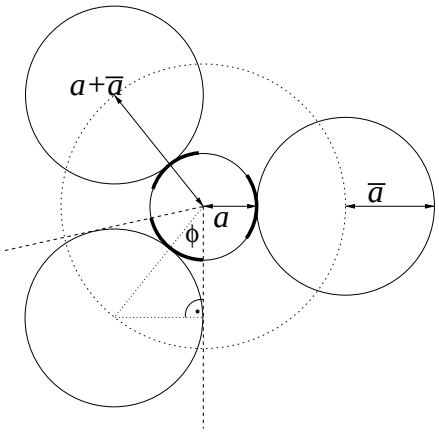

Fig. 1. Schematic graph of a central particle with radius a, surrounded by identical particles of the mean radius $\overline{a}$. The shielded surface of the center particle is shown as thick solid arcs.

(circumference) of a particle (in 2D). Thus, the expected mean coordination number becomes

$$\overline{C} = \int_0^\infty da\ C(a)\ f(a) = \pi c_s q_0\ , \tag{10}$$

with $q_0 = \int_0^\infty\ da\ \ f(a)/\phi(a)$. Note that Eqs. (9) and (10) imply that $C(a)$ is linear in a (with an offset) – this can be false for much broader particle size distribution than examined here. In the same spirit, according to Eq. (10), the trace of the fabric for a polydisperse assembly is

$$\langle F_{\alpha\alpha}\rangle_V = \overline{C}\nu g_2\ , \tag{11}$$

with our central result, the correction factor

$$g_2 = \frac{\langle a^2\rangle_g}{\overline{a^2}} = \frac{\int_0^\infty\ da\ a^2 f(a)/\phi(a)}{q_0 \int_0^\infty\ da\ a^2\ f(a)}\ , \tag{12}$$

and $\overline{C}\ = \langle C\rangle$ implied. The brackets $\langle a^k\rangle_g$ denote the k-th moment of the modified distribution $f(a)/\phi(a)$, normalized by q_0. This leads to $\langle a^0\rangle_g\ = 1$ and for a monodisperse granulate, one has again $g_2 = 1$. In our nomenclature, g_k thus means $\langle a^k\rangle_g$ normalized by $\overline{a^k}$.

In the limit of a narrow size distribution, by Taylor expansion to first order in ϵ (corresponding to a Taylor expansion around $a = \overline{a}$), one obtains

$$\frac{1}{\phi(a)} \approx \frac{1}{\phi_1(a)} = \frac{6}{\pi}\left(1 + \frac{\sqrt{3}}{\pi}\epsilon\right) \ . \tag{13}$$

In Fig. 2, we plot $1/\phi(a)$ from Eq. (8) and its Taylor expansion in Eq. (13). The dashed line on the graph is the approximation and the solid curve is the exact form. Since the simpler approximation has less than 1% error in the range $-0.5 < \epsilon < 1.5$ (or $0.5 < a/\overline{a} < 2.5$), we will use it for correspondingly narrow size distributions in the following. By this approximation, one obtains the correction factor for the fabric of a polydisperse packing,

$$g_2 \approx 1 + \frac{\sqrt{3}}{\pi}\left(\frac{\overline{a^3}}{\overline{a}\overline{a^2}} - 1\right) \ , \tag{14}$$

which accounts for arbitrary size distribution functions $f(a)$, as long as they are not too wide.

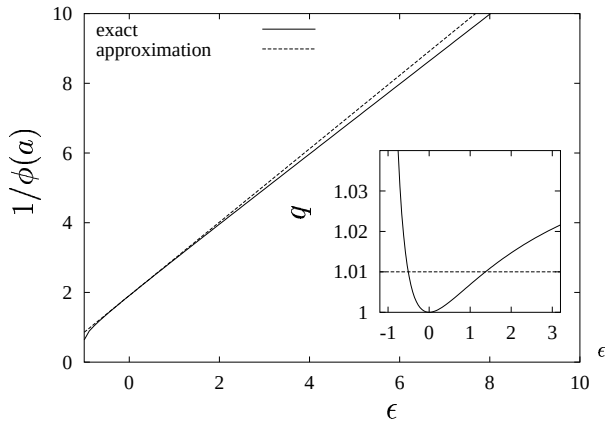

Fig. 2. $1/\phi(a)$ plotted against $\epsilon = a/\overline{a} - 1$, in first order approximation and exact. The inset shows the quality factor $q = \phi(a)/\phi_1(a)$ of the approximation.

3.4 Special size distributions

In this section, we apply the above theory to special cases in order to evaluate the quality of Eq. (14) in the following section.

3.4.1 Bidisperse

In a bidisperse system, one has two particle radii a_1 and a_2 and the size-distribution function is thus

$$f(a) = f_1\delta(a - a_1) + f_2\delta(a - a_2) \ , \tag{15}$$

with the fractions $f_1 = N_1/N$ and $f_2 = N_2/N$, of particles with radius a_1 and a_2, respectively, with $N = N_1 + N_2$. It is straightforward to compute the terms necessary for a calculation of g_2 in both Eqs. (12) and (14) one by one. Combining the terms

$$\begin{aligned}
\overline{a} &= f_1 a_1 + f_2 a_2 \ , \\
\overline{a^2} &= f_1 a_1^2 + f_2 a_2^2 \ , \\
\overline{a^3} &= f_1 a_1^3 + f_2 a_2^3 \ , \\
q_0 &= f_1\phi(a_1)^{-1} + f_2\phi(a_2)^{-1} \ , \\
q_0\langle a^2\rangle_g &= f_1 a_1^2\phi(a_1)^{-1} + f_2 a_2^2\phi(a_2)^{-1} \ , \text{ and} \\
\phi(a_{1,2}) &= \arcsin\left[1/(1 + a_{1,2}/\overline{a})\right] \ ,
\end{aligned}$$

allows the calculation of both the exact expression and the approximate one. For a special bidisperse system with $a_1 = a$, $a_2 = 3a$, and $f_1 = f_2 = 1/2$, i.e. $\epsilon_1 = -\frac{1}{2}$ and $\epsilon_2 = \frac{1}{2}$, we are in the range where our approximation, Eq. (14), has less than about 1% error, see Fig. 2. Therefore, for this special bidisperse situation, one gets

$$\begin{aligned}
\overline{a} &= 2a \ , \\
\overline{a^2} &= 5a^2 \ , \\
\overline{a^3} &= 14a^3 \ , \\
q_0 &= (\phi(a_1)^{-1} + \phi(a_2)^{-1})/2 \ , \text{ and} \\
q_0\langle a^2\rangle_g &= (a^2\phi(a_1)^{-1} + 9a^2\phi(a_2)^{-1})/2 \ , \text{ with} \\
\phi(a_1) &= \arcsin\left[1/(1 + 1/2)\right] = \arcsin\left(2/3\right) , \text{ and} \\
\phi(a_2) &= \arcsin\left[1/(1 + 3/2)\right] = \arcsin\left(2/5\right) .
\end{aligned}$$

After explicit computation this leads to the exact $g_2 = 1.223$ or to $g_2 \approx 1.220$ from Eq. (14), in good agreement with the exact value for a binary mixture with size ratio $a_2/a_1 = 3$.

3.4.2 Uniform disperse

In a uniform disperse system, a special case of polydisperse systems, the radius of the particles is distributed uniformly between $(1-w_0)\overline{a}$ and $(1+w_0)\overline{a}$ where

$2w_0\overline{a}$ is the width of size-distribution function

$$f(a) = \frac{1}{2w_0\overline{a}}\Theta\left((1+w_0)\overline{a} - a\right)\Theta\left(a - (1-w_0)\overline{a}\right), \tag{16}$$

with the Heaviside step function $\Theta(x) = 1$ for $x \geq 0$ and $\Theta(x) = 0$ elsewhere. It is again straightforward to compute the contributions to g_2, so that one obtains

$$\begin{aligned}
\overline{a^2} &= (1/3)\overline{a}^2(3+w_0^2)\ , \\
\overline{a^3} &= \overline{a}^3(1+w_0^2)\ , \\
q_0 &= \frac{1}{2w_0}\int_{1-w_0}^{1+w_0}\frac{dx}{\arcsin(1/(1+x))}\ , \\
q_0\langle a^2\rangle_g &= \frac{\overline{a}^2}{2w_0}\int_{1-w_0}^{1+w_0}\frac{dx\ x^2}{\arcsin(1/(1+x))}\ , \text{ and} \\
g_2 &= \frac{3\int_{1-w_0}^{1+w_0}\frac{dx\ x^2}{\arcsin(1/(1+x))}}{(3+w_0^2)\int_{1-w_0}^{1+w_0}\frac{dx}{\arcsin(1/(1+x))}}\ .
\end{aligned}$$

The polydispersity correction for $w_0 = 0.5$, leads to $g_2 = 1.085$, while from the approximation one gets $g_2 = 1.083$, both again in good agreement.

4 Simulations and Results

For a numerical verification of our theoretical predictions, we perform soft sphere molecular dynamics (MD) simulations of disks in a box with flat walls. The interaction of the particles is the simplest linear spring-dashpot model, see e.g. (Luding et al., 1994; Luding, 1997), disregarding friction and non-linear behavior at the contact. Firstly, we generate about $N = 2000$ particles (disks), on a sparse square lattice, with random radii according to the distribution function of radii $f(a)$, as defined above, and give them some small initial velocity, in order to create initial disorder. Secondly, we use the MD simulation and compress the system until a pre-defined volume fraction, say $\nu = 0.9$, is reached. In most cases, compression is achieved by moving the top-wall down. However, also other protocols of compression like a stress-controlled isotropic compression did not lead to a recognizably difference in the initial condition – the lack of friction is the likely reason for this independence on the history of preparation. Then the simulation is continued until almost all kinetic energy is dissipated. Figure 3 shows one typical steady state configuration. Averages are performed in the middle of the system, in order to avoid boundary effects,

i.e. we do not use the cells close to the boundaries displayed in Fig. 3. The center-subsystem can be divided further into various smaller subsystems to allow for different averages of varying quality. Within the statistical fluctuations, the system is spatially homogeneous, and the majority of the overlaps detected is smaller than a few per-cent of the particle diameter, even for the highest densities used.

For the comparison with theory, the average of the trace of the fabric tensor, the average of the contact number, and the g_2 factor are computed directly from the simulations center-sub-systems using Eq. (14).

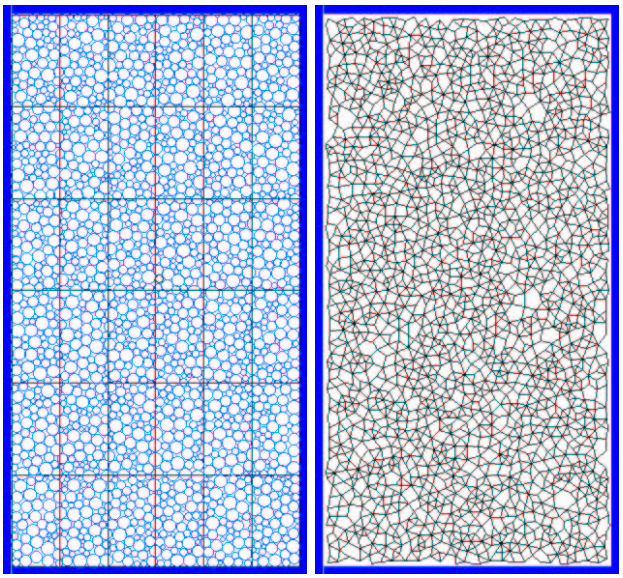

Fig. 3. Typical uniform disperse configuration with $w_0 = 0.5$. (Left) Particles are plotted as circles and the straight lines indicate the subsystems. (Right) Contact network.

First, we examine the probability distribution of the orientation, θ, of the fabric tensor, i.e. the orientation of the eigenvector that corresponds to the major eigenvalue. Fig. 4(a) shows the polar plot of the distribution of angles θ. Fig. 4(b) is similar to (a), only the angles of the branch vectors ϕ for each contact are used to compute the probability distribution. These two graphs show that the system in static equilibrium is almost isotropic and hence has no memory about its previous compression. The compression was performed vertically, but a small majority of orientations is found at $\theta \approx \pi/2$. We applied several different uniaxial compression protocols, but the homogeneity of the system remains – within about 10 per-cent fluctuations. There is no indication of a correlation between the applied strain and the response of the fabric tensor. We attribute this fact to the lack of friction in our model; if friction is present, one expects memory effects, i.e. a dependence of $p(\theta)$ on the history of the construction of the packing, see (Dubujet and Dedecker, 1998; Radjai et al., 1998, 1999).

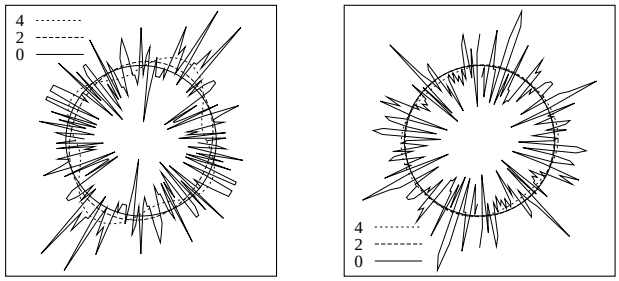

(a) (b)

Fig. 4. Polar plot of the distributions $p(\theta)$ (a), where θ is given by the orientation of the major eigendirection of the fabric tensor, and $p(\phi)$ (b), where ϕ is given by the orientations of the branch vectors between two particles in contact.

In order to quantify the deviation from an isotropic packing, we perform Fourier series fits of the form

$$p(\theta) = p_0 + p_2 \sin(2\theta + \theta_2) + p_4 \sin(4\theta + \theta_4) \ , \tag{17}$$

shown in Fig. 4 as lines (the maximum order of the fit is given in the inset). Order 2 means, for example, that all terms higher than order 2 are neglected. For the distribution $p(\theta)$, one obtains for the order 4 fit, $p_2/p_0 = -0.07$ and $p_4/p_0 = 0.15$, whereas one has systematically smaller deviation from isotropy, i.e. $p_2/p_0 = -0.04$ and $p_4/p_0 = 0.02$, for $p(\phi)$.

4.1 Bidisperse

The parameters for the bidisperse size-distribution are the same as in subsection 3.4.1. First the simulation results are compared to our theoretical predictions. We divide the center system (disregarding the boundary subsystems) into 16 subsystems and calculate $\langle F_{\alpha\alpha} \rangle_V$, g_2, $\overline{C}$, and ν for five different simulations with different initial configurations. Fig. 5 shows $\langle F_{\alpha\alpha} \rangle_V$ plotted against $\overline{C}\nu g_2$, where the line indicates the identity. The simulation data fluctuate around the theoretically expected curve.

Therefore, using $x = \langle F_{\alpha\alpha} \rangle_V / \overline{C}\nu g_2$, we compute the mean, $\langle x \rangle = (1/n) \sum x$, and the typical fluctuations, $\sigma_x = \sqrt{\langle x^2 \rangle - \langle x \rangle^2}/(n-1)$, for different numbers of subsystems n. Fig. 6 shows the error plotted against the number of subsystems. It increases with increasing number of subsystems or for decreasing number of particles in the sample, as displayed in the inset. The data show that the error of a measurement depends on the size of the averaging volume or representative elementary volume (REV). The relative fluctuations of one measurement are of the order of one per-cent for 70 particles averaged over, proportional to M^{-1} when M is the number of particles in the subsystem. The

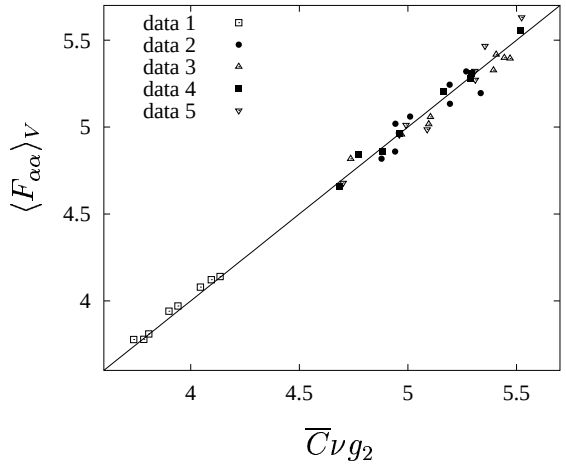

Fig. 5. Average of the trace of the fabric tensor plotted against $\overline{C}\nu g_2$ for bidisperse systems from five different realizations. The solid line is the theoretically expected relation, see Eq. (11). Data set 1 has a density of $\nu = 0.84$, whereas the density of the other data sets is $\nu = 0.90$.

second important fact can be extracted from the other inset, namely from the plot of $\langle x\rangle$ vs. M, where one can see that the theory slightly underestimates the true contact number density. In conclusion, $\langle x\rangle$ is independent of the number of subsystems, but its error increases with M, or tends to practically zero for large enough subsystems.

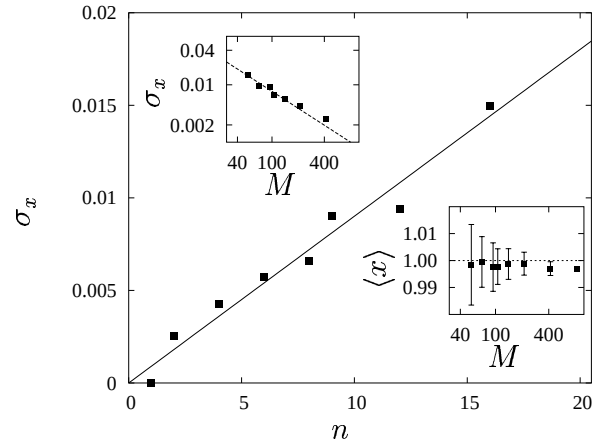

Fig. 6. The error σ_x of $\overline{C}\nu g_2/\langle F_{\alpha\alpha}\rangle_V$ for different numbers of subsystems n. The line is a fit to the data $\sigma_x \approx 9\,10^{-4}\,n$. The insets shows the same data plotted against the number of particles M in the subsystems. The top inset gives the error with the fit $\sigma_x \approx 0.7M^{-1}$ (dashed line), the bottom inset gives the average $\langle x\rangle$, which should be unity (dotted line), and the error-bars indicate the fluctuations of the n different values. .

Second, the g_2 factor calculated from the simulations is compared to the theoretically expected value. In the total system, the particle size distribution is defined according to Eq. (15) with $f(a_1) = f(a_2) = \frac{1}{2}$. But when taking the average in subsystems, the values of $f(a_1)$ and $f(a_2)$ differ. It is straightfor-

ward to rewrite Eq. (14) as

$$g_2 = 1 - \frac{\sqrt{3}}{\pi}\left(1 - \frac{14 - 13\ \Delta f}{(2 - \Delta f)(5 - 4\ \Delta f)}\right)\ , \tag{18}$$

where g_2 is a function of $\Delta f = f(a_2) - f(a_1)$ and it will be equal to the global value 1.220 only when Δf equals zero. When g_2 is plotted against Δf for different simulations, as expected, one recovers the theoretical approximation Eq. (18), indicating that the fluctuations in Figs. 5 and 6 are of statistical origin.

4.2 Uniform disperse

The parameters for the bidisperse size-distribution are the same as in subsection 3.4.2. Here, we generate the particles with uniformly distributed radii, see Eq. (16). In Fig. 7, $\langle F_{\alpha\alpha}\rangle_V$ is plotted against $\overline{C}\nu g_2$. Again we observe fluctuations around the theoretically expected values. As mentioned before, the scatter in the data is due to the averaging over finite samples. The slight underestimation maybe due to a limited validity of our assumptions, or due to the overlap that is not taken into account.

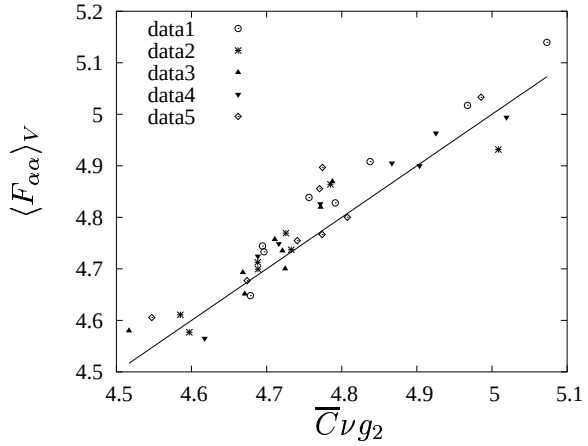

Fig. 7. The plot as in Fig. 5 for uniform disperse systems with global density $\nu = 0.9$.

4.2.1 Coordination number and compacity

In our preparation procedure, the system size is fixed at the desired value such that a constant density is achieved. This implies that below the minimal possible density (uniform disperse size distribution) $\nu_0 \approx 0.837 \pm 0.002$, no

stable contact network could be obtained for the frictionless systems considered here. Note that the issue of a maximum random packing density of a bi- or polydisperse sphere packing is still subject of onging research, see e.g. Liu and Ha (2002); Luding (2002b) and references therein. Therefore, we present data only at higher densities in the following.

For the uniform disperse size-distribution, we check the basic assumption of our theory, namely that c_s does not depend on the particle size. In Fig. 8, the values of c_s are plotted for different densities and different particle sizes. We notice that c_s is constant for the larger densities, but slightly decreases with particle size for lower densities. This implies that our analysis could be somewhat less accurate in dilute systems, however, within the fluctuations of the data due to the finite size of the samples, we conclude that the assumption $c_s = \text{const.}$ is reasonable.

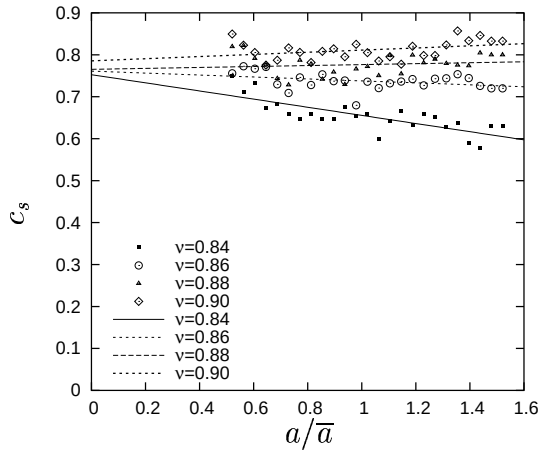

Fig. 8. Linear compacity, see Eq. (9), for different particle sizes and different densities. The lines are line-fits to the data with offset $c_0 \approx 0.780$, 0.765, 0.795, 0.800, and slope $c_m \approx -0.09$, -0.04, -0.02, 0.005, for increasing density. Only for low densities close to the stability threshold the assumption fails.

In Fig. 9, the contact number is plotted for different sizes and for different system densities. The data show that the smallest possible particles will have a coordination number of approximately $C(a \to 0) \approx 2$ and that the increase of coordination number with the particle size is slightly increasing with the density. Thus, we expect also the mean coordination number to increase slightly with density due to the finite stiffness of the particles that allow for additional contacts when the density is increasing. Our results for different densities are in qualitative agreement with the simulations by Kruyt and Rothenburg, see Fig. 9 in the paper by (Kruyt and Rothenburg, 2001). Note that coordination numbers $C(a) < 4$ are frequently observed, while $\overline{C} \geq 4$ is valid for these frictionless systems.

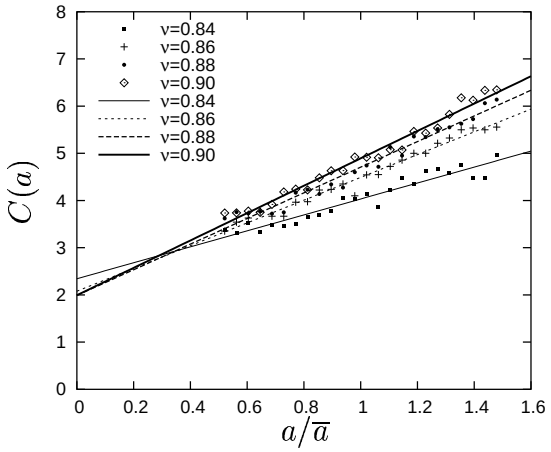

Fig. 9. Contact number for different particles sizes and different densities. The lines are line-fits ($c_0 + c_m a/\overline{a}$) to the data with offset $c_0 \approx 2.35$, 2.14, 2.16, 2.08, and slope $c_m \approx 1.69$, 2.20, 2.46, 2.75, for increasing density.

4.2.2 Local size distribution

In Fig. 10, the g_2 factor is plotted for the different subsystems from the five different realizations. The line is the theoretically expected value, however, the simulation results are fluctuating around it. We attribute the variation of g_2 again to the local size distribution function within one subsystem, which is different from the global distribution function. In the following, the local g_2 will be used.

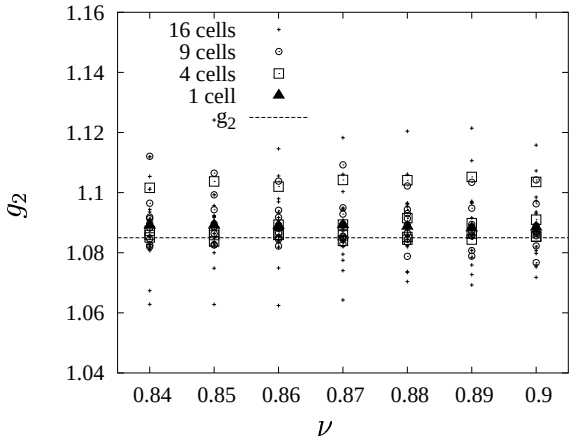

Fig. 10. The g_2 factor from uniform disperse simulations, plotted against the global density in the system from which it was taken.

4.2.3 Variable density

In Fig. 11, the trace of the fabric tensor $\langle F_{\alpha\alpha} \rangle_V$ is plotted against $\overline{C}\nu g_2$ from simulations with different volume fractions and a uniform disperse particle size distribution. The agreement between the data and the theoretical prediction is

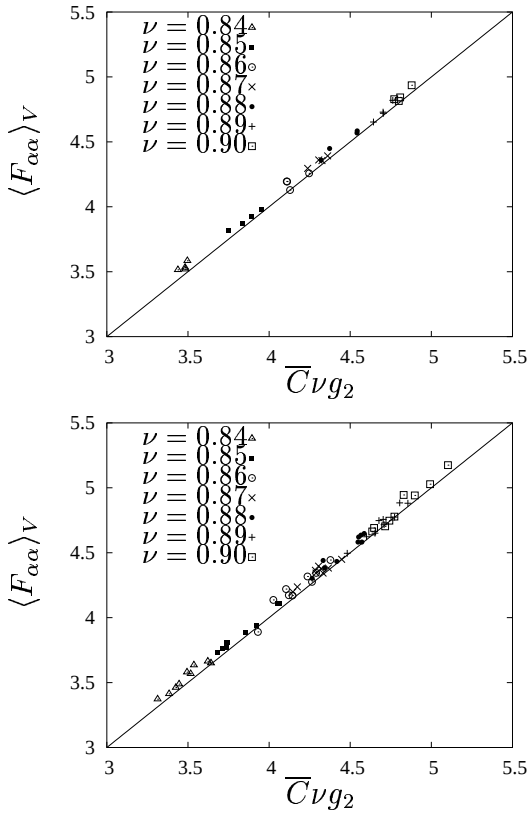

Fig. 11. The same data as in Fig. 5, but for uniform disperse particles with different volume fractions $0.84 \leq \nu \leq 0.90$. The two figures are for four and nine subsystems evaluated.

reasonable also for smaller densities $\nu < 0.90$, as used above. With decreasing density ν, the trace of the fabric tensor also decays, but remains on the identity line. Hence our theoretical correction factor g_2 works for bi- and uniform-disperse particle size distribution functions likewise.

In Fig. 12, the probability distribution of the direction of the branch vectors is plotted for different densities. Like in the bidisperse case, there is no evidence for anisotropy in the packing.

4.3 Coordination number and overlap

In Fig. 13, the coordination number in the center cells is plotted against the density obtained in these cells. Note that the density in the center cell is somewhat larger than the global density due to the empty spaces between the wall and those particles contacting it. The larger the number of subsystems and the smaller the global density, the larger are the fluctuations in both $\overline{C}$ and ν. Even unphysical values $\overline{C} < 4$ can be obtained due to our evaluation procedure that involves also so-called "rattlers", i.e. particles with no contacts that do

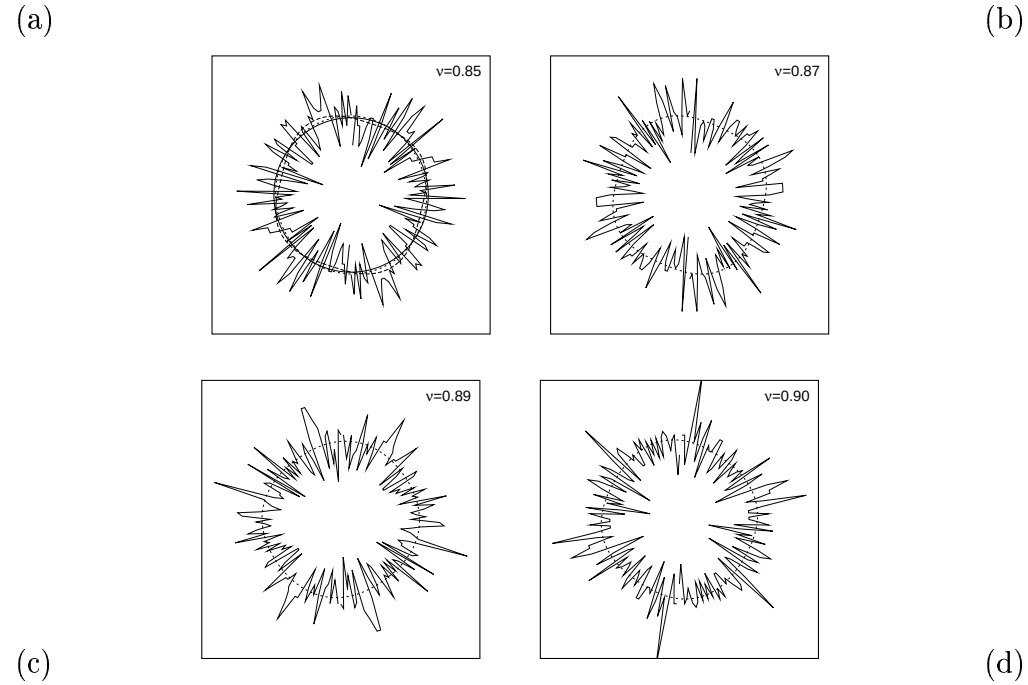

Fig. 12. Polar plot of $p(\phi)$ for the orientation of the branch vector for global volume fractions (a) $\nu = 0.85$, (b) $\nu = 0.87$, (c) $\nu = 0.89$, and (d) $\nu = 0.90$.

not contribute to the mechanically stable contact-network. The coordination number rapidly increases from a value $C \approx 4$ at the smallest density. However, within the scope of this paper, an evaluation of the functional behavior is postponed and we do not examine this quantity further.

As the final plot, we present the mean dimensionless overlap as a function of the global density for the simulations presented above, in Fig. 14. We remark that the typical overlap obtained is only about 2.5 per-cent of the particle radius for $\nu = 0.91$, and that the overlap increases linearly from zero, at the minimal density $\nu_c \approx 0.84$.

5 Conclusion and Discussion

In summary, the trace of the fabric tensor was examined in almost isotropic, disordered arrays of polydisperse, frictionless particles in static equilibrium, at different densities. The key result is an analytical expression for the contact number density, i. e. the trace of the fabric tensor. It factorizes into three contributions: (i) the volume fraction (or, with other words, the density), (ii) the mean coordination number (a function of density), and (iii) a dimensionless correction factor g_2, which is only dependent on the particle size probability distribution function. The theoretical prediction for g_2 is verified with molecular dynamics simulations for various size distributions and densities. As long as

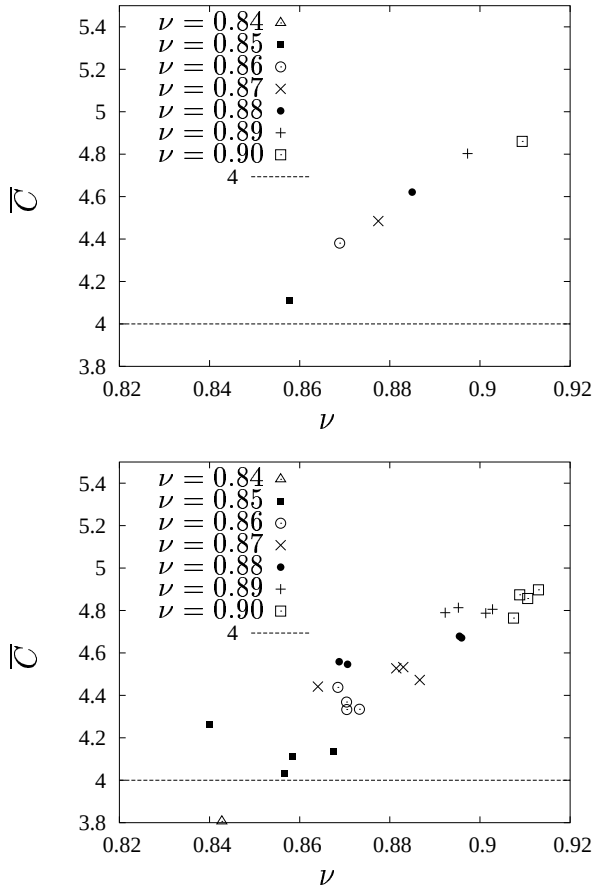

Fig. 13. Plot of the mean coordination number as function of the density. The different data sets are obtained from one cell and from four center cells.

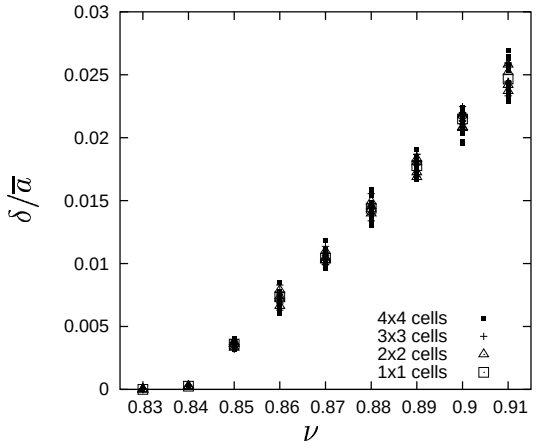

Fig. 14. Plot of the dimensionless overlap as a function of the global density with $\delta/\overline{a} \propto (\nu - \nu_c)$.

the distribution is reasonably narrow the agreement between theory and simulation is reasonable, within the statistical fluctuations. The latter issue was also addressed in more detail, and a typical deviation of about one per-cent from the mean is obtained for averaging volumes containing around 100 par-

ticles. Preliminary simulations with anisotropic configurations and frictional particles show that the results still hold within a few per-cent (for the cases examined, however, larger differences can be expected for strongly different protocols of preparation of the sample). Even though friction should reduce the average number of contacts for the same preparation protocol, the density would also be reduced at the same time. Thus there is hope that our relations still hold as function of density. In any case, we expect that our results are a starting point for studies involving more realistic systems and particles.

The trace of the fabric tensor is a quantity that is related to the bulk stiffness of the material, see (Rothenburg and Selvadurai, 1981; Chang, 1988; Lätzel et al., 2000; Kruyt and Rothenburg, 2001; Luding, 2002a). Our theoretical prediction relates it to the first three moments of the size distribution function (in the case of a sufficiently narrow size distribution), and thus allows to predict a macroscopic material property based on a microscopic property of the material. The prediction is that, in general, the trace of the fabric – and with it the bulk stiffness – will increase with g_2, a function of the "width" of the size distribution.

Preliminary studies, concerning the trace of the stress tensor for systems with different particle sizes, $\langle\sigma_{\alpha\alpha}\rangle_V$, show that it contains a lowest order correction factor dependent on the first two moments of $f(a)$, i.e. $\langle\sigma_{\alpha\alpha}\rangle_V \propto (\overline{a^2}/\overline{a}^2 - 1)$.

Future work, concerns the correction for the fabric and the pressure also for broader polydisperse size distributions, and for three-dimensions. Furthermore, the presented results should be generalized towards an-isotropic structures and frictional, cohesive and possibly non-spherical particles.

Acknowledgements

We are grateful to Hans J. Herrmann and Niels P. Kruyt for inspiring discussions and acknowledge the financial support from the Deutsche Forschungsgemeinschaft (DFG).

References

Allen, M. P. and Tildesley, D. J. (1987). *Computer Simulation of Liquids.* Oxford University Press, Oxford.

Bagi, K. (1996). Stress and strain in granular assemblies. *Mech. of Materials*, 22:165–177.

Bagi, K. (1999). Microstructural stress tensor of granular assemblies with volume forces. *J. Appl. Mech.*, 66:934–936.

Bagi, K. (2003). Statistical analysis of contact force components in random granular assemblies. *Granular Matter*, 5:45–54.

Ball, R. C. and Blumenfeld, R. (2002). Stress field in granular systems: Loop forces and potential formulation. *Phys. Rev. Lett.*, 88:115505.

Bathurst, R. J. and Rothenburg, L. (1988). Micromechanical aspects of isotropic granular assemblies with linear contact interactions. *J. Appl. Mech.*, 55:17–23.

Bauer, E. and Tejchman, J. (1995). Numerical study of the effect of grain rotations on material behavior in a fault zone. In *Mechanics of Jointed and Faulted Rock*, pages 317–322.

Bigoni, D. and Loret, B. (1999). Effects of elastic anisotropy on strain localization and flutter instability in plastic solids. *J. of the Mechanics & Physics of Solids*, 47(7):1409.

Cambou, B., Dubujet, F., Emeriault, F., and Sidoroff, F. (1995). Homogenization for granular materials. *Eur. J. Mech. A/Solids*, 14(2):255–276.

Cambou, B. and Sidoroff, F. (1985). State description of a granular material through static internal variables from a discrete analysis. *Journal de Mecanique Theorique et Appliquee*, 4(2):223.

Chang, C. S. (1988). Micromechanical modelling of constitutive relations for granular media. In *Micromechanics of granular media*, Amsterdam. Elsevier.

Chang, C. S., Chao, S. J., and Chang, Y. (1995). Estimates of elastic moduli for granular material with anisotropic random packing structure. *Int. J. Solids & Structures*, 32(14):1989–2009.

Cowin, S. C. (1985). The relationship between the elasticity tensor and the fabric tensor. *Mechanics of Materials*, 4(2):137–147.

Cowin, S. C. (1998). Imposing thermodynamic restrictions on the elastic constant-fabric relationship. *Journal of Biomechanics*, 31:759.

Cundall, P. A. and Strack, O. D. L. (1979). A discrete numerical model for granular assemblies. *Géotechnique*, 29(1):47–65.

Cundall, P. A. and Strack, O. D. L. (1983). Modeling of microscopic mechanisms in granular materials. In Jenkins, J. T. and Satake, M., editors, *Mechanics of Granular Materials: New Models and Constitutive Relations*, pages 137–149, Amsterdam. Elsevier.

Darve, F., Flavigny, E., and Meghachou, M. (1995). Yield surfaces and principle of superposition: revisit through incrementally non-linear constitutive relations. *International Journal of Plasticity*, 11(8):927.

Dedecker, F., Chaze, M., Dubujet, P., and Cambou, B. (2000). Specific features of strain in granular materials. *Mech. Coh.-Fric. Mat.*, 5(3):174–193.

Dubujet, P. and Dedecker, F. (1998). Micro-mechanical analysis and modelling of granular materials loaded at constant volume. *Granular Matter*, 1(3):129–136.

Edwards, S. F. and Grinev, D. V. (1999). Statistical mechanics of stress transmission in disordered granular arrays. *Phys. Rev. Lett.*, 82:5397–5400.

Ehlers, W. and Müllerschön, H. (2000). Parameter identification for a macroscopic granular soil model applied to dense Berlin sand. *Granular Matter*,

2:105–112.

Emeriault, F. and Chang, C. S. (1997). Interparticle forces and displacements in granular materials. *Computers and Geotechnics*, 20(3/4):223–244.

Goddard, J. D. (1986). Microstructural origins of continuum stress fields - a brief history and some unresolved issues. In DeKee, D. and Kaloni, P. N., editors, *Recent Developments in Structered Continua. Pitman Research Notes in Mathematics No. 143*, page 179, New York. Longman, J. Wiley.

Goddard, J. D. (1998). Continuum modeling of granular assemblies. In Herrmann, H. J., Hovi, J.-P., and Luding, S., editors, *Physics of Dry Granular Media*, pages 1–24, Dordrecht. Kluwer Academic Publishers.

Gudehus, G. (1996). A comprehensive constitutive equation for granular materials. *Soils and Foundations*, 36(1):1–12.

Guyon, E., Roux, S., Hansen, A., Bideau, D., Troadec, J.-P., and Crapo, H. (1990). Non-local and non-linear problems in the mechanics of disordered systems: application to granular media and rigidity problems. *Rep. Prog. Phys.*, 53:373–419.

Herrmann, H. J. and Luding, S. (1998). Modeling granular media with the computer. *Continuum Mechanics and Thermodynamics*, 10:189–231.

Jacobs, D. J. (1998). Generic rigidity in three-dimensional bond-bending networks. *J. Phys. A: Math. Gen.*, 31:6653.

Jaeger, H. M., Nagel, S. R., and Behringer, R. P. (1996). Granular solids, liquids, and gases. *Reviews of Modern Physics*, 68(4):1259–1273.

Jenkins, J. T. (1997). Inelastic behavior of random arrays of identical spheres. In Fleck, N. A. and Cocks, A. C. E., editors, *IUTAM Symposium on Mechanics of Granular and Porous Materials*, pages 11–22. Kluwer Academic Publishers.

Kolymbas, D., Herle, I., and von Wolffersdorff, P. A. (1995). Hypoplastic constitutive equation with internal variables. *Int. J. for Numerical and Analytical Methods in Geomechanics*, 19:415–436.

Kruyt, N. P. and Rothenburg, L. (1996). Micromechanical definition of strain tensor for granular materials. *ASME Journal of Applied Mechanics*, 118:706–711.

Kruyt, N. P. and Rothenburg, L. (2001). Statistics of the elastic behavior of granular materials. *Int. J. of Solids and Structures*, 38:4879–4899.

Kuhl, E., D´Addetta, G. A., Herrmann, H. J., and Ramm, E. (2000). A comparison of discrete granular material models with continuous microplane formulations. *Granular Matter*, 2:113–121.

Kun, F. and Herrmann, H. J. (2000). Damage development under gradual loading of composites. *J. Mater. Sci.*, 35(18):4685–4693.

Lätzel, M., Luding, S., and Herrmann, H. J. (2000). Macroscopic material properties from quasi-static, microscopic simulations of a two-dimensional shear-cell. *Granular Matter*, 2(3):123–135. cond-mat/0003180.

Lätzel, M., Luding, S., and Herrmann, H. J. (2001). From discontinuous models towards a continuum description. In Vermeer, P. A., Diebels, S., Ehlers, W., Herrmann, H. J., Luding, S., and Ramm, E., editors, *Continuous*

and Discontinuous Modelling of Cohesive Frictional Materials, pages 215–230, Berlin. Springer.

Liao, C.-L. and Chang, T.-C. (1997). A generalized constitutive relation for a randomly packed particle assembly. *Computers and Geotechnics*, 20(3/4):345–363.

Liao, C.-L., Chang, T.-P., Young, D.-H., and Chang, C. S. (1997). Stress-strain relationship for granular materials based on the hypothesis of best fit. *Int. J. Solids & Structures*, 34:4087–4100.

Liu, S. J. and Ha, Z. Y. (2002). Prediction of random packing limit for multimodal particle mixtures. *Powder Technology*, 126(6):283–296.

Luding, S. (1997). Stress distribution in static two dimensional granular model media in the absence of friction. *Phys. Rev. E*, 55(4):4720–4729.

Luding, S. (2002a). From microscopic simulations to macroscopic material behavior. *Computer Physics Communications*, 147:134–140.

Luding, S. (2002b). Liquid-solid transition in bi-disperse granulates. *Advances in Complex Systems*, 4(4):379–388.

Luding, S. (2004). Micro-macro transition for anisotropic, periodic, elastic solids. in preparation.

Luding, S., Clément, E., Blumen, A., Rajchenbach, J., and Duran, J. (1994). Anomalous energy dissipation in molecular dynamics simulations of grains: The "detachment effect". *Phys. Rev. E*, 50:4113.

Luding, S. and Herrmann, H. J. (2001). Micro-macro transition for cohesive granular media. in: Bericht Nr. II-7, Inst. für Mechanik, Universität Stuttgart, S. Diebels (Ed.).

Luding, S., Lätzel, M., and Herrmann, H. J. (2001a). From discrete element simulations towards a continuum description of particulate solids. In Levy, A. and Kalman, H., editors, *Handbook of Conveying and Handling of Particulate Solids*, pages 39–44, Amsterdam, The Netherlands. Elsevier.

Luding, S., Lätzel, M., Volk, W., Diebels, S., and Herrmann, H. J. (2001b). From discrete element simulations to a continuum model. *Comp. Meth. Appl. Mech. Engng.*, 191:21–28.

Mehrabadi, M. M., Nemat-Nasser, S., Shodja, H. M., and Subhash, G. (1988). Some basic theoretical and experimental results on micromechanics of granular flow. In *Micromechanics of granular media*, Amsterdam. Elsevier.

Moukarzel, C. (1996). An efficient algorithm for testing the generic rigidity of graphs in the plane. *J. Phys. A: Math. Gen.*, 29:8079.

Oda, M. and Iwashita, K. (2000). Study on couple stress and shear band development in granular media based on numerical simulation analyses. *Int. J. of Enginering Science*, 38:1713–1740.

Oda, M., Iwashita, K., and Kazama, H. (1997). Micro-structure developed in shear bands of dense granular soils and its computer simulation – mechanism of dilatancy and failure –. In Fleck, N. A. and Cocks, A. C. E., editors, *IUTAM Symposium on Mechanics of Granular and Porous Materials*, pages 353–364. Kluwer Academic Publishers.

Oda, M. and Kazama, H. (1998). Microstructure of shear bands and its re-

lation to the mechanism of dilatancy and failure of dense granular soils. *Géotechnique*, 48(4):465–481.

Ouchiyama, N. and Tanaka, T. (1981). Porosity of a mass of solid particles having a range of sizes. *Ind. Eng. Chem. Fund.*, 20(1):66–71.

Radjai, F., Roux, S., and Moreau, J. J. (1999). Contact forces in a granular packing. *Chaos*, 9(3):544.

Radjai, F., Wolf, D. E., Jean, M., and Moreau, J.-J. (1998). Bimodal character of stress transmission in granular packings. *Phys. Rev. Lett.*, 80(1):61–64.

Rothenburg, L. and Selvadurai, A. P. S. (1981). A micromechanical definition of the Cauchy stress tensor for particulate media. In Selvadurai, A. P. S., editor, *Mechanics of Structured Media*, pages 469–486. Elsevier, Amsterdam.

Roux, J.-N. (1997). Contact disorder and nonlinear elasticity of granular packings: a simple model. In Behringer, R. P. and Jenkins, J. T., editors, *Powders & Grains 97*, pages 215–218, Rotterdam. Balkema.

Roux, J.-N. (2000). On the geometric origin of mechanical properties of granular materials. cond-mat/0001246.

Roux, S., Hild, F., Fokwa, D., Breysse, D., Geymonat, G., and Pijaudier-Cabot, G. (1991). Current-conductance and stress-elastic modulus correlations. *Journal de Physique II*, 1(3):265.

Roux, S., Stauffer, D., and Herrmann, H. J. (1987). Simulation of disordered systems of cylinders. I. Geometrical behavior. *J. Physique*, 48:341–345.

Sadd, M. H., Gao, J., and Shukla, A. (1997). Numerical analysis of wave propagation through assemblies of elliptical particles. *Computers and Geotechnics*, 20(3/4):323–344.

Sadegh, A. M., Cowin, S. C., and Luo, G. M. (1991). Inversions related to the stress-strain-fabric relationship. *Mechanics of Materials*, 11(4):323.

Shima, S. (1993). Behaviour of assembly of particles during compaction process in relation to constitutive equation. In *The first Nisshin Engineering Particle Technology International Seminar: Discrete Particle Simulations in Powder Technology*, page 32, Osaka, Japan.

Tejchman, J. (2002). Patterns of shear zones in granular bodies. *Acta Mechanica*, 155:1–2.

Thornton, C. (1997). Force transmission in granular media. *KONA Powder and Particle*, 15:81–90.

Thornton, C. (2000). Numerical simulations of deviatoric shear deformation of granular media. *Géotechnique*, 50(1):43–53.

Thornton, C. and Antony, S. J. (2000). Quasi-static deformation of a soft particle system. *Powder Technology*, 109(1-3):179–191.

Thornton, C. and Randall, C. W. (1988). Applications of theoretical contact mechanics to solid particle system simulation. In *Micromechanics of granular media*, Amsterdam. Elsevier.

Tobita, Y. (1997). Importance of incremental nonlinearity in the deformation of granular materials. In Fleck, N. A. and Cocks, A. C. E., editors, *IUTAM Symposium on Mechanics of Granular and Porous Materials*, pages 139–150. Kluwer Academic Publishers.

Tsoungui, O., Vallet, D., Charmet, J.-C., and Roux, S. (1998). "partial pressures" supported by granulometric classes in polydisperse granular media. *Phys. Rev. E*, 57(4):4458–4465.

Vardoulakis, I., Labuz, J. F., Papamichos, E., and Tronvoll, J. (1998). Continuum fracture mechanics of uniaxial compression on brittle materials. *Int. J. Solids & Structures*, 35(31-32):4313.

Vardoulakis, I. and Sulem, J. (1995). *Bifurcation analysis in geomechanics.* hapman & Hall, London.

Vermeer, P. A., Diebels, S., Ehlers, W., Herrmann, H. J., Luding, S., and Ramm, E., editors (2001). *Continuous and Discontinuous Modelling of Cohesive Frictional Materials*, Berlin. Springer. Lecture Notes in Physics 568.

Wolf, D. E. and Grassberger, P., editors (1997). *Friction, Arching and Contact Dynamics.* World Scientific, Singapore.